

An experimental study of steel fiber-reinforced high-strength concrete slender columns under cyclic loading



Karen E. Caballero-Morrison, J.L. Bonet*, Juan Navarro-Gregori, Pedro Serna-Ros

Instituto de Ciencia y Tecnología del Hormigón, Universitat Politècnica de València, Camino de Vera s/n, 46022 Valencia, Spain

ARTICLE INFO

Article history:

Available online 11 August 2012

Keywords:

Slender column
Confined concrete
High-strength concrete
Steel fiber
Ductility
Cyclic load

ABSTRACT

Structural engineers usually limit the use of HSC columns to seismic active zones because of their brittle behavior in comparison with NSC, even though it presents advantages both in terms of mechanics and durability. A possible solution to improve the ductile behavior of HSC columns is the use of transverse reinforcement and steel fibers simultaneously.

In addition, the use of HSC makes the design of more slender columns possible, with the consequent increase of second-order effects. However, there are few experimental tests on columns of medium slenderness (between 5 and 10) subjected to cyclic loads including or excluding steel fibers.

This article presents experimental research work on the behavior of slender columns subjected to combined constant compression and cyclic lateral loads. Fifteen tests were carried out in order to study the behavior of such elements.

The following variables were studied: concrete strength, slenderness, axial load level, transverse reinforcement ratio, and volumetric steel-fiber ratio. The maximum load and deformation capacity of the columns were analyzed. The fact that the inclusion of steel fibers into the concrete mixture increases the deformation capacity was verified. Moreover, a minimum transverse reinforcement is required in order to improve the effectiveness of the steel fibers with no significant decrease in the carrying capacity under cyclic loading. The inclusion of steel fibers in HSC can ensure similar ductility values to those of NSC. It was shown that slenderness influences the deformation capacity.

© 2012 Elsevier Ltd. All rights reserved.

1. Introduction

In recent years, the use of high-strength concrete (HSC) in construction has increased and been accepted by designers and builders. The immediate benefits of using this type of concrete in columns focus on increasing the load capacity and material savings, and result in smaller cross-sections, and more slender columns, with the consequent increase of second-order effects.

Currently, the criterion of capacity-based design [13,14] guaranteeing that plastic hinges appear in the beam ends and in the bottom of first-storey columns or bridge columns. Thus, reinforced concrete columns have to provide a significant inelastic response with a minor decrease of load capacity without a significance loss of load capacity.

Since the behavior of high-strength concrete in columns is more brittle than that of normal-strength concrete [21,16], its use is gradually being accepted in seismic zones [20]. In order to guarantee a ductile behavior of the columns, and therefore their safety, design codes [11,13,1] include a minimum transverse

reinforcement ratio. In general, this ratio is proportional to the concrete strength and the axial load level among other variables. HSC columns require a greater transverse reinforcement ratio than NSC ones, and this makes concrete casting difficult, especially for high axial load levels. Transverse reinforcement improves the column ductility, and its ability to absorb and dissipate energy without a significant loss of load capacity under accidental actions. Another solution for the improvement of the column ductility is adding steel fibers to the concrete mixture [26]. The combined use of steel fibers and transverse reinforcement can reduce the transverse reinforcement ratio required by codes, especially for the case of seismic design [6]. However, code proposals neglect the favorable effect of steel fibers [13,1].

Several authors, including [17,22,7] have studied the behavior of fiber-reinforced high-strength concrete. These studies show the typical stress–strain constitutive relationships of concrete in compression, in which the inclusion of steel fibers represents a minor increase in the peak stress, a significant increase in strain at peak stress, and a substantial increase in toughness. Recent research [15,2,29,8,27] has shown that the presence of steel fibers delays concrete spalling, and increases the deformation capacity of concrete columns subjected to compressive axial load and constant eccentricity.

* Corresponding author. Tel.: +34 96 387 7007x75615; fax: +34 96 387 7569.
E-mail address: jlbonet@cst.upv.es (J.L. Bonet).

There are numerous publications concerning the study of the strength and deformation capacity of columns under cyclic loading [5,9]. Experimental tests available focus on reinforced concrete columns (without fibers) with shear slenderness (λ_V) under 6.5 [25]. There are some laboratory tests of steel fiber-reinforced concrete columns subjected to combinations of axial and lateral loads [6].

Second-order effects (P – Δ effect) have a significant influence on the deformation capacity of slender columns [3], and there are a few tests on columns with slenderness over 6.5 only for normal-strength concrete [6]. As a result, it is necessary to study the behavior of HSC columns subjected to constant axial load combined with cyclic lateral loads.

This research work presents an experimental program on the behavior of slender normal-strength and high-strength concrete columns, under constant compression and cyclic loads, with and without steel fibers. The effect of confinement and the presence of steel fibers are studied through the following variables: axial load level, concrete strength, and slenderness of the column. These results can be used to calibrate numerical models, and to validate simplified methods included in codes.

2. Test program

Test specimens were designed to represent two semi-columns of two adjacent storeys connected by a stub. The geometric details of the specimens are shown in Fig. 1, and the cross-section details of the semi-columns are shown in Fig. 2. This type of specimen has been previously employed by Yamashiro and Sies [37], Priestley and Park [28], and Barrera et al. [4] among others.

The following parameters were analyzed: (a) the shear slenderness ($\lambda_V = L_s/h = M/(V \cdot h)$, where h was the total depth of the cross-section, M and V were the bending moment and the shear load applied); (b) the relative normal force ($v = N/[b \cdot h \cdot f_c]$, where N was the axial load applied, b was the width of the cross-section, and f_c was the concrete compressive strength); (c) the confinement effectiveness of the transverse reinforcement ($\alpha \cdot \omega_{\omega}$, where α was the confinement effectiveness factor, this factor takes into account the spacing and the arrangement of the stirrups in the section, and ω_{ω} was the volumetric transverse reinforcement ratio [13] Section 5.4.3.2.2 (8)); and (d) the steel fiber content.

In the experimental program each parameter studied ranges as follows:

- Concrete strength (f_c). Nominal strengths of 30 and 75 MPa were chosen.
- Relative normal force (v). The following three levels were considered: 0.10 and 0.35.
- Shear slenderness ratio (λ_V). Values of 5.77 and 10.71 were taken into account. Second-order effects cannot be neglected in either case, and the values chosen are greater than those included in the literature.
- Longitudinal reinforcement ratio (ρ_l). Two similar values were considered: 1.44% if $\lambda_V = 10.71$ and 1.74% if $\lambda_V = 5.77$.

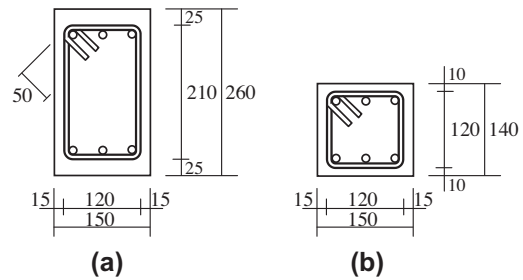


Fig. 2. Cross-section details (unit: mm).

- Effective volumetric mechanical ratio of confinement ($\alpha \cdot \omega_{\omega}$). Three levels were taken into account: high (0.05), medium (0.02), and low (0.01). Given a transverse reinforcement diameter $\phi_t = 8$ mm: (a) $\alpha \cdot \omega_{\omega} = 0.05$ was obtained for HSC assuming a transverse reinforcement spacing (s_t) of 50 mm if $\lambda_V = 5.77$, and $s_t = 70$ mm if $\lambda_V = 10.71$, and for NSC with $s_t = 100$ mm if $\lambda_V = 5.77$; (b) $\alpha \cdot \omega_{\omega} = 0.02$ was obtained for HSC with $s_t = 100$ mm if $\lambda_V = 5.77$; and (c) $\alpha \cdot \omega_{\omega} = 0.01$ taking $s_t = 600$ mm if $\lambda_V = 5.77$ for both HSC and NSC. The latter level is considered for analysis if it is possible to replace the transverse reinforcement with steel fibers, for cases with larger volume of steel fibers.
- Steel fiber content: 30 and 60 kg/m³, corresponding to volumetric steel-fiber ratios of 0.38% and 0.76% respectively.

Table 1 shows the details of the 15 specimens included in the experimental program.

All specimens were tested at 28 days. To determine the average concrete compressive strength three cylinders (150 × 300 mm) [31] were tested for each specimen (see Table 1).

2.1. Material properties

Cement Portland CEM I 52,5R [33], and crushed limestone gravel with sizes ranging from 4 to 7 mm were used. The dosages considered are listed in Table 2.

The steel used was B 500 SD [11], and C class [12]. The results of the characterization tests following UNE EN-10002-1 [30] are shown in Fig. 3. To determine the average values of the steel mechanical properties two pieces of reinforcing steel were tested for each nominal diameter.

The steel fibers used were DRAMIX RC-65/35-BN, with aspect ratio $l/d = 35/0.55 = 63.63$, and 1100 MPa tensile strength for NSC, and DRAMIX RC-80/40-BP, with aspect ratio $l/d = 40/0.50 = 80$, and 2800 MPa tensile strength for HSC. A greater tensile strength for HSC has been chosen to ensure that the failure is due to a loss of bond-slip in the steel fibers, because the bond strength between steel fibers and concrete increases with the concrete strength. A 550 × 150 × 150 mm prismatic specimen was made for each mixture, and a 3-point bending test was performed complying with

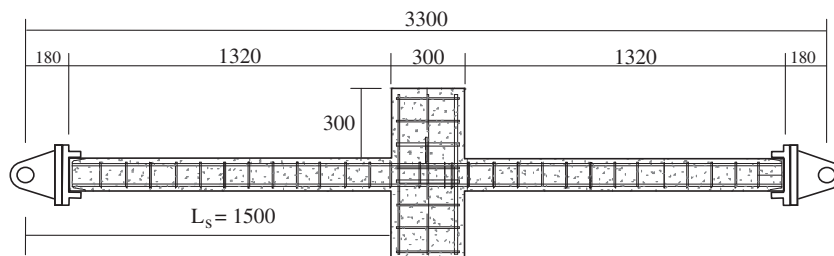


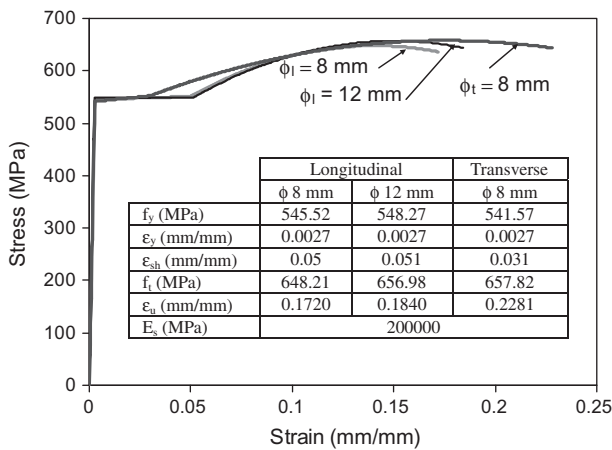
Fig. 1. Dimensions of test specimens (unit: mm).

Table 1
Details of test specimens.

Id	Specimen	h (m)	b (m)	f_c (MPa)	Steel fiber content (kg/m ³)	λ_V	N (kN)	$\frac{N}{b h f_c}$	Reinforcement				
									Longitudinal		Transverse ($\phi_t = 8$ mm)		
									ϕ_l (mm)	ρ_l (%)	s_t (mm)	ρ_s (%)	$\alpha \cdot \omega_{\omega}$
N1	HF00L05V2S100	0.26	0.15	64.10	0	5.77	895.1	0.36	6 ϕ 12	1.74	100	1.40	0.02
N2	HF00L05V2S50	0.26	0.15	71.70	0	5.77	959.0	0.34	6 ϕ 12	1.74	50	2.79	0.06
N3	HF00L05V1S50	0.26	0.15	75.40	0	5.77	294.7	0.11	6 ϕ 12	1.74	50	2.79	0.05
N4	HF00L10V1S70	0.14	0.15	70.50	0	10.71	175.2	0.12	6 ϕ 8	1.44	70	3.03	0.05
N5	HF30L05V2S600	0.26	0.15	75.60	30	5.77	967.7	0.33	6 ϕ 12	1.74	600	0.23	0.01
N6	HF60L05V2S100	0.26	0.15	75.50	60	5.77	1013.3	0.34	6 ϕ 12	1.74	100	1.40	0.02
N7	HF60L05V2S50	0.26	0.15	79.20	60	5.77	1056.7	0.34	6 ϕ 12	1.74	50	2.79	0.05
N8	HF60L05V2S600	0.26	0.15	75.10	60	5.77	993.7	0.34	6 ϕ 12	1.74	600	0.23	0.01
N9	HF60L05V1S50	0.26	0.15	81.10	60	5.77	333.9	0.11	6 ϕ 12	1.74	50	2.79	0.05
N10	HF60L10V1S70	0.14	0.15	79.30	60	10.71	190.2	0.11	6 ϕ 8	1.44	70	3.03	0.04
N11	HF60L10V2S70	0.14	0.15	79.10	60	10.71	598.8	0.36	6 ϕ 8	1.44	70	3.03	0.04
N12	NF00L05V2S100	0.26	0.15	33.57	0	5.77	491.7	0.38	6 ϕ 12	1.74	100	1.40	0.04
N13	NF30L05V2S100	0.26	0.15	33.37	30	5.77	473.8	0.36	6 ϕ 12	1.74	100	1.40	0.04
N14	NF60L05V2S100	0.26	0.15	33.65	60	5.77	412.7	0.31	6 ϕ 12	1.74	100	1.40	0.04
N15	NF60L05V2S600	0.26	0.15	32.12	60	5.77	420.6	0.34	6 ϕ 12	1.74	600	0.23	0.01

Table 2
Concrete dosages considered (kg/m³).

Description	Concrete type	Cement	Water	Sand	Crushed limestone	Steel fibers	Silica fume	Plasticizer 651N	Pozzolith	Superplasticizer Glenium AC31
NSC	1	348	220	1065	666	–	–	–	–	–
	2					30	–	1.22 (%)	–	2.44 (%)
	3					60	–	1.57 (%)	–	3.13 (%)
HSC	4	427.5	180	705	890	–	50	4.27 (%)	–	8.55 (%)
	5					30	50	5.34 (%)	–	10.69 (%)
	6					60	50	6.41 (%)	–	12.82 (%)

**Fig. 3.** Stress–strain behavior of steel.

UNE-EN 14651:2007 [32] in order to determine the corresponding limit of proportionality (f_{li}) and the residual flexural tensile strength of fiber reinforced concrete corresponding to Crack Mouth Opening Displacement (CMOD) = CMOD_j (f_{Rj} , for $j = 1-4$ [18]) (see Table 3).

2.2. Test setup

A steel-loading frame was designed to perform the tests, as shown in Fig. 4a. The horizontal loading system comprises a 2500 kN hydraulic actuator (Fig. 4b), which is part of a frame. The lateral loading system was fixed to an auxiliary frame that transmitted lateral loads to the test slab (Fig. 4c). The lateral load was applied to the specimen using a 500 kN double effect hydraulic jack.

The forces applied by the hydraulic actuators were controlled by two load cells: a 2000 kN cell, attached to a plate in the horizontal loading system frame, and a 500 kN cell, between the specimen and the hydraulic actuator of the lateral load system.

More detailed information on the test setup, instrumentation, and test procedure can be found in Caballero-Morrison et al. [6].

2.3. Instrumentation

Strain gauges were placed in eight sections at only one side of the specimen (Fig. 5). To ensure that the instrumented side was the first to reach failure, an additional longitudinal bar was positioned at a distance greater than the potential length of the plastic hinge in the top and in the bottom faces.

To measure displacements 15 LVDTs were used. Devices 1–10 recorded the lateral displacement of the specimen (Fig. 6). The rotation of the central element (stub) was obtained from the records of devices 7 and 8. LVDT 11 recorded the transverse displacement of the specimen due to possible geometric imperfections or lateral instability (Fig. 6), even though this effect was observed as negligible during the tests even when the damage level was very high. LVDTs 12–15 (Fig. 7a and b), were designed to indirectly record the average bending curvature at 70 mm and at 170 mm from the column-stub interface.

2.4. Test procedure

First, a constant horizontal load corresponding to the relative normal force was applied, and next the cyclic lateral load. The first load cycle was carried out with load-control until the total bending moment (M_{cs}) was 75% of the ultimate bending moment (M_u) at the critical section (at 70 mm from the column-stub interface, see Fig. 8) in each direction of the tip displacement (Δ_1^+ and Δ_1^-). The ultimate bending moment (M_u) was calculated

Table 3
Results of 3-point bending tests.

Id	Specimen	f_L (MPa)	$f_{R,1}$ (MPa)	$f_{R,2}$ (MPa)	$f_{R,3}$ (MPa)	$f_{R,4}$ (MPa)
N6	HF30L05V2S600	4.41	5.20	7.66	7.15	5.87
N7	HF60L05V2S100	5.20	9.59	11.86	10.01	8.11
N8	HF60L05V2S50	6.99	11.29	12.89	11.42	10.20
N9	HF60L05V2S600	5.00	12.53	14.64	12.52	11.28
N10	HF60L05V1S50	5.75	11.05	15.11	14.46	11.50
N11	HF60L10V1S70	5.92	12.21	14.27	13.61	12.24
N12	HF60L10V2S70	5.20	9.41	10.49	9.25	7.08
N13	NF30L05V2S100	2.89	2.89	2.90	2.91	2.91
N14	NF60L05V2S100	4.41	6.51	7.24	7.18	6.37
N15	NF60L05V2S600	4.35	6.59	7.80	7.46	6.58

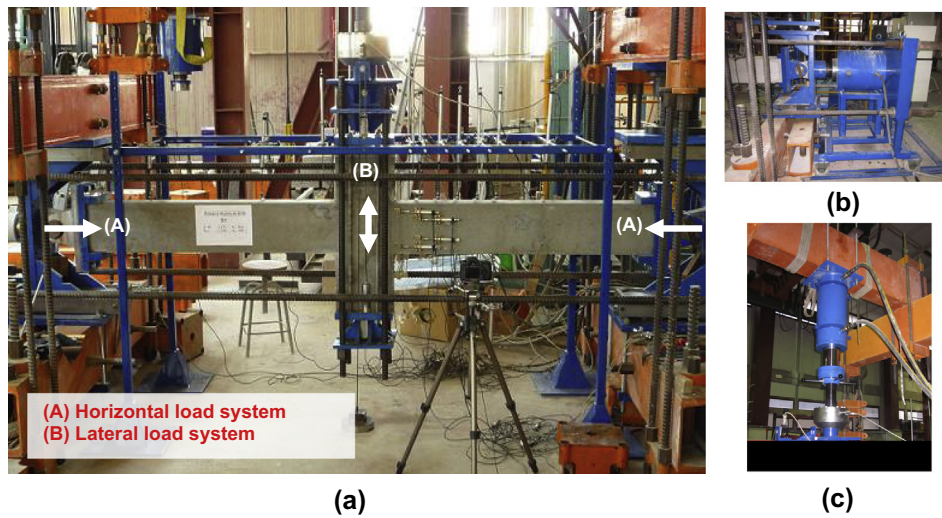


Fig. 4. Photograph of experimental setup and testing frame.

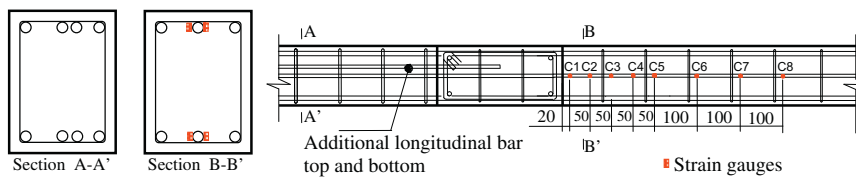


Fig. 5. Top view of the strain gauges disposal (unit: mm).

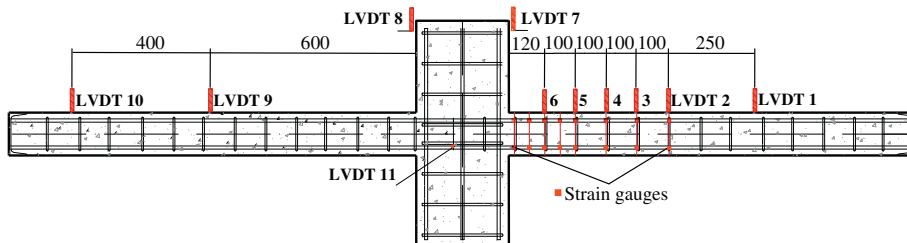


Fig. 6. Lateral displacement measurements (unit: mm).

following EC-2 [12]. This took into account the properties of the materials and the axial force pre-applied. The effect of confinement of concrete and steel fibers was neglected, and no safety factors were considered. During the first cycle, it was possible to obtain the maximum and minimum displacements at the ends

of the column (Δ_1^+ and Δ_1^- , at $0.75 \cdot M_u$ and $-0.75 \cdot M_u$, respectively, Fig. 9). The nominal elastic displacement Δ_y was calculated on the basis of the following expression [16]:

$$\Delta_y = \frac{4}{3} \cdot \frac{\Delta_1^+ + |\Delta_1^-|}{2} \tag{1}$$

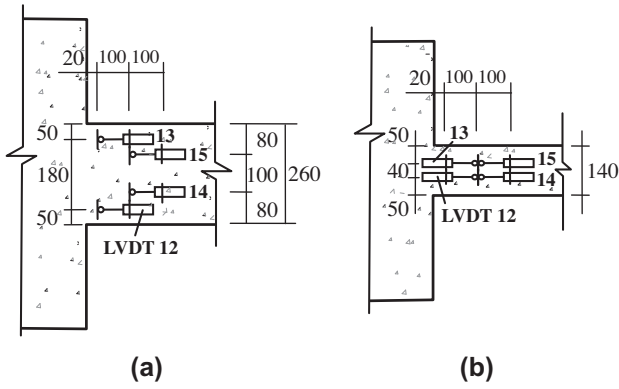


Fig. 7. Horizontal displacement measurements (unit: mm).

All the other cycles were carried out with load–displacement control by imposing a displacement of $\Delta = \mu \cdot \Delta_y$, where μ was the nominal displacement ductility factor. Thus, at the beginning of the second cycle $\mu = 1$, and then Δ increased Δ_y every two cycles [16] (Fig. 9). Fig. 8 shows how to calculate Δ displacement at the end of the column and the total bending moment (M_{cs}) at the critical section.

A conventional failure criterion was fixed in all tests, assuming a 20% loss of strength capacity in terms of lateral load or bending moment [16,26].

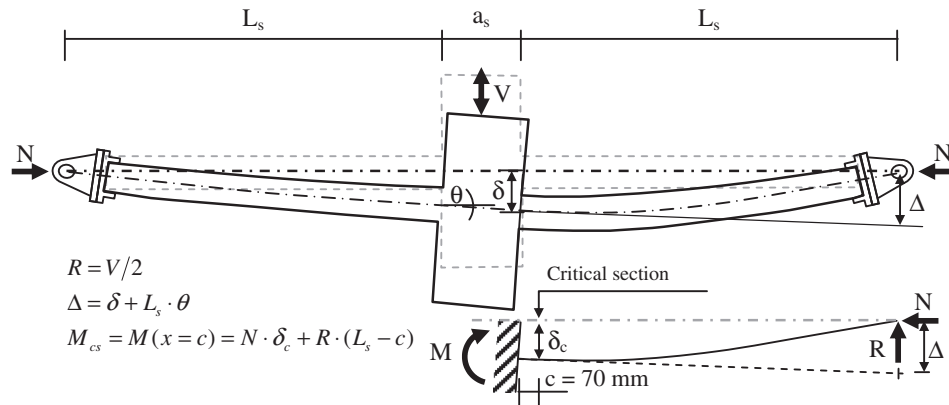


Fig. 8. Idealization of specimen.

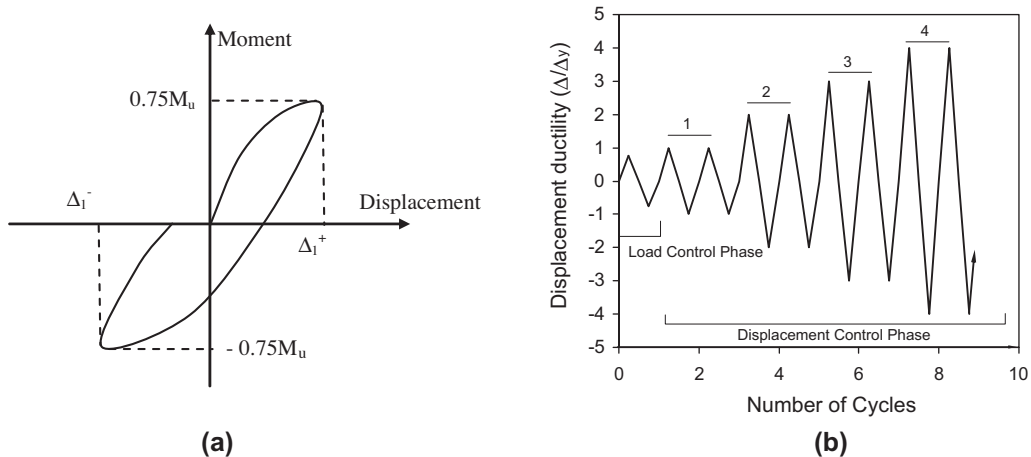


Fig. 9. Test procedure: (a) determination of Δ_1^+ and Δ_1^- from the first elastic cycle load control, (b) loading history.

3. Test results and observations

Figs. 10 and 11 show the load–displacement diagrams recorded, and Table 4 shows a summary of the main test results.

3.1. General behavior

The following general observations were made:

1. Concrete cover spalled in all specimens (Figs. 10 and 11). In HSC specimens spalling (Fig. 12a) was due to the development of splitting cracks in the concrete surrounding the longitudinal reinforcement [10]. With the addition of fibers, this effect diminishes (Fig. 12a vs. d and b vs. e) and concrete did not clearly spall, except in the cases of NF60L05V2S600, HF30L05V2S600, and HF60L05V2S600, with 600 mm stirrup spacing (Fig. 12c and f).
2. The longitudinal reinforcement yielded in all NSC and HSC specimens (Figs. 10 and 11).
3. The critical region length l_{cr} of each column specimen was evaluated following the physical observation method proposed by Pam and Ho [24]. Regarding the l_{cr}/h ratio (critical region length l_{cr} over the total depth of the section (h)), it was observed that it increased with the slenderness, the axial force applied, and the transverse reinforcement spacing, and decreased with the inclusion of steel fibers (Table 4). This ratio was similar for NSC and HSC columns. This length (l_{cr}) ranged between $0.54 \cdot h$

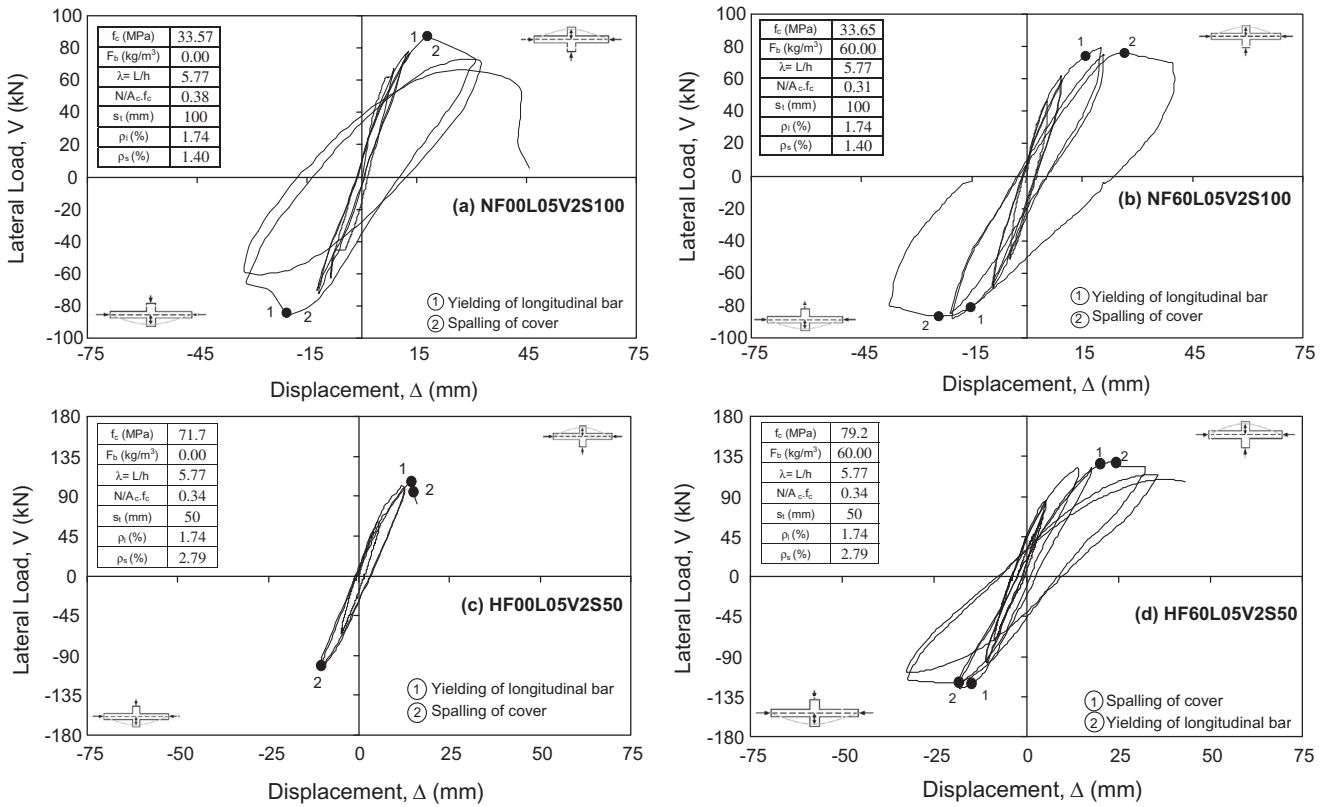


Fig. 10. Lateral load vs. tip displacement: effect of concrete strength and steel fibers.

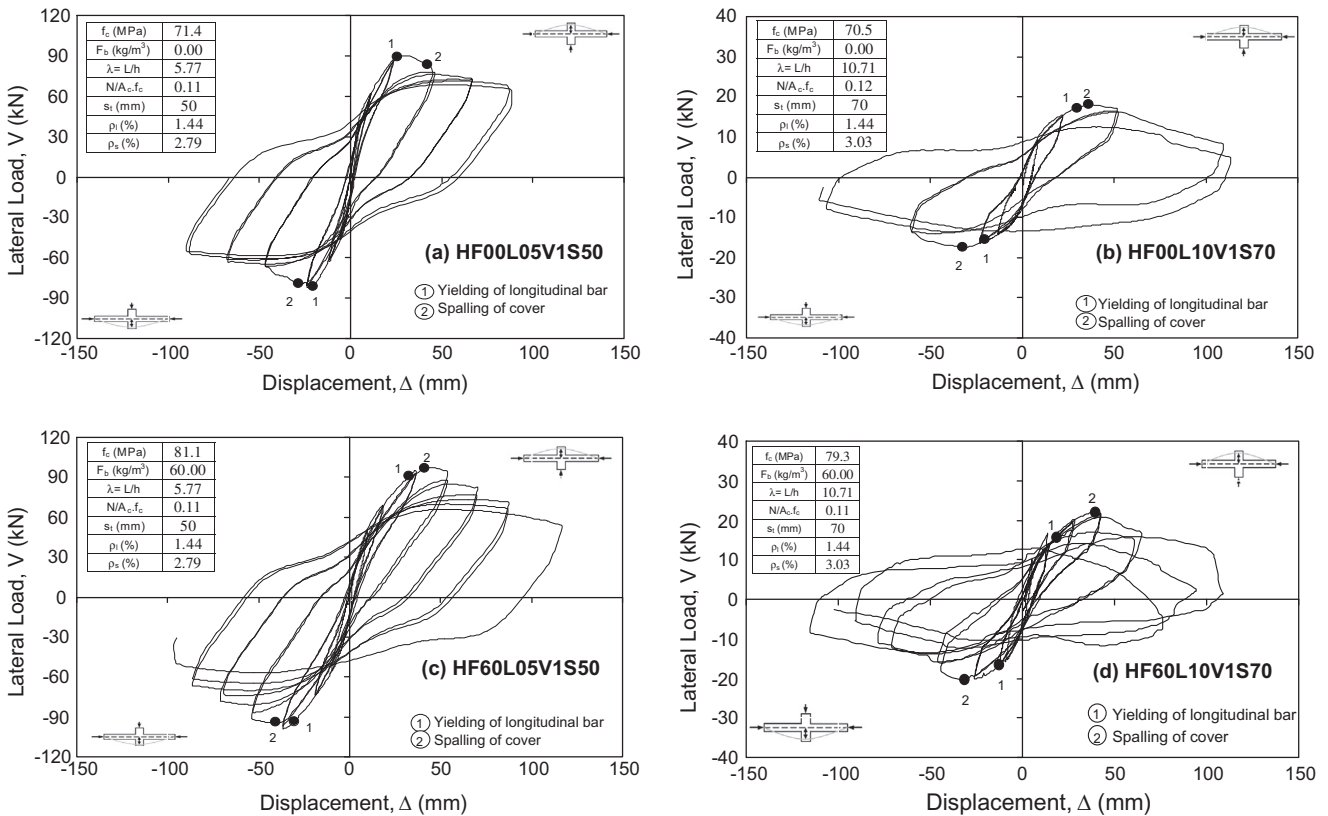


Fig. 11. Lateral load vs. tip displacement. HSC: effect of slenderness and steel fibers.

Table 4
Summary of test results.

Id	Specimen	μ	Bar buckling	Critical region l_{cr} (m)	l_{cr}/h
N1	HF00L05V2S100	2	Yes	0.50	1.92
N2	HF00L05V2S50	2	–	0.23	0.88
N3	HF00L05V1S50	5	Yes	0.36	1.38
N4	HF00L10V1S70	3	–	0.20	1.43
N5	HF30L05V2S600	2	Yes	0.30	1.15
N6	HF60L05V2S100	2	Yes	0.30	1.15
N7	HF60L05V2S50	3	Yes	0.22	0.85
N8	HF60L05V2S600	2	Yes	0.34	1.31
N9	HF60L05V1S50	6	Yes	0.14	0.54
N10	HF60L10V1S70	6	–	0.20	1.43
N11	HF60L10V2S70	2	Yes	0.19	1.36
N12	NF00L05V2S100	2	Yes	0.35	1.35
N13	NF30L05V2S100	2	Yes	0.20	0.77
N14	NF60L05V2S100	3	Yes	0.24	0.92
N15	NF60L05V2S600	2	Yes	0.35	1.35

(for $\lambda_V = 5.77$ and $\nu = 0.10$) and $1.92 \cdot h$ (for $\lambda_V = 5.77$ and $\nu = 0.35$).

- Nonfibrous specimens suffered major damage (Fig. 12a and b), and cracks orientation is vertical in most cases. In fibrous specimens the crack distribution showed greater smearing (Fig. 12d and e), with the exception of specimens with $s_t = 600$ mm, these were NF60L05V2S600, HF30L05V2S600 and HF60L05V2S600. In these a typical shear failure occurred after stirrup yielding, spalling of concrete cover, and buckling of the longitudinal bars (Fig. 12c and f).
- The section connecting the stub and the semi-column was not damaged in most specimens (stub effect), despite being subjected to the maximum bending moment (Fig. 12). According to other authors [26,19] this fact is explained by the confinement effect caused by the stub in the nearby sections. For this reason, the critical section was positioned 70 mm away from the stub within the critical region zone (Fig. 8). Therefore, the moment – curvature diagram is calculated at 70 mm from the column-stub interface.
- While nonfibrous HSC columns subjected to medium axial load level ($\nu = 0.35$) did not show post-peak behavior (Fig. 10c), the inclusion of steel fibers improved it markedly (Fig. 10d).

- It was found that buckling of the longitudinal reinforcement had an important influence on the deformation capacity of the column. This occurred when the reinforcement yielded (since this significantly decreased the stiffness of the reinforcement), and the concrete cover spalled. Rebar buckling was observed in the following cases:

- In the columns with $\lambda_V = 5.77$, with an axial load level of $\nu = 0.35$, without fibers, for NSC and HSC, and with $s_t = 100$ mm and $s_t = 600$ mm. In these cases the nominal ductility μ achieved was 2. The presence of steel fibers significantly delayed rebar buckling in NSC specimens (between $\mu = 2$ and $\mu = 3$), and slightly in HSC specimens. The effect of the inclusion of steel fibers in HSC was less favorable than in NSC due to a previous development of splitting cracks in the plane defined by the longitudinal reinforcement, which generated a weak plane. However, if the transverse reinforcement spacing s_t decreased to 50 mm, in nonfibrous HSC columns the longitudinal reinforcement did not suffer buckling ($\mu = 2$), and with fibers it occurred at a higher ductility ($\mu = 3$).
- In the columns with $\lambda_V = 5.77$, and axial load $\nu = 0.10$, with or without fibers, for HSC. The longitudinal reinforcement buckled at a nominal ductility μ between 5 and 6.
- In the specimen HF60L10V2S70, with $\lambda_V = 10.71$, axial load $\nu = 0.35$, with fibers, with $s_t = 70$ mm, and with HSC. In this case the nominal ductility μ achieved was 2. None of the specimens suffered buckling for a level of axial load $\nu = 0.10$.

To sum up, the longitudinal reinforcement did not buckle in the following specimens: HF00L05V2S50, HF00L10V1S70, and HF60L10V1S70.

Therefore, the occurrence of buckling of the longitudinal reinforcement in compression depends on the ductility achieved, the type of concrete (NSC and HSC, with or without fibers), the axial load level, the diameter of the longitudinal reinforcement, and the transverse reinforcement spacing. EC-8 [13] includes different transverse reinforcement spacings to achieve the ductility required to prevent bars from buckling after concrete cover spalls ($8 \cdot \phi_l$ for DCM and $6 \cdot \phi_l$ for DCH, where ϕ_l is lowest diameter of the reinforcement in compression). However, ACI-318 (08) [1] considers a

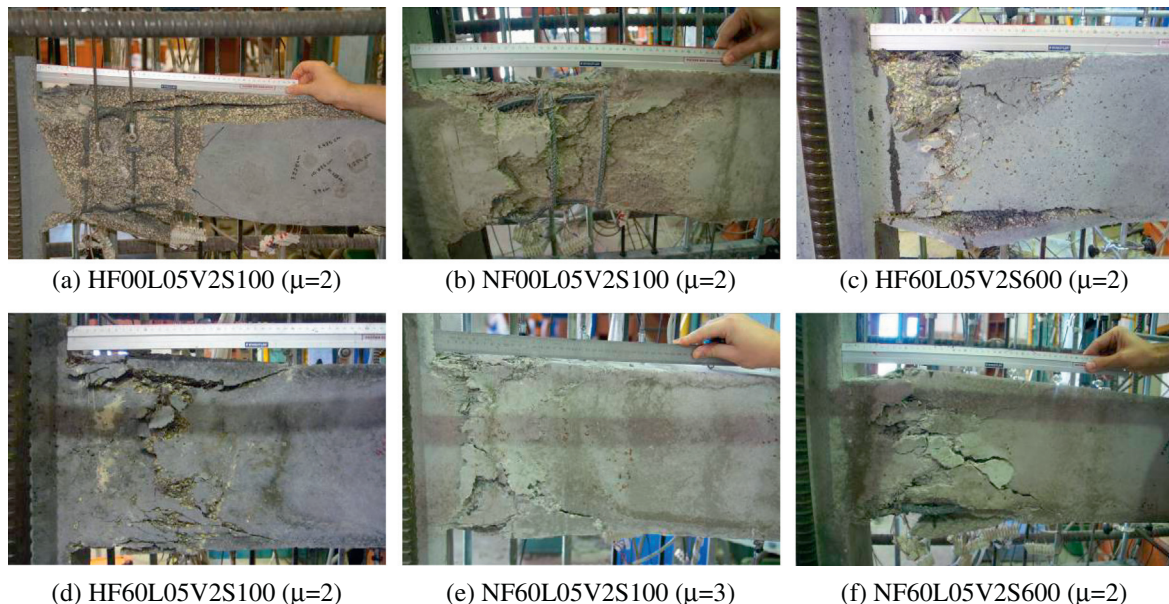


Fig. 12. Specimen behavior at failure.

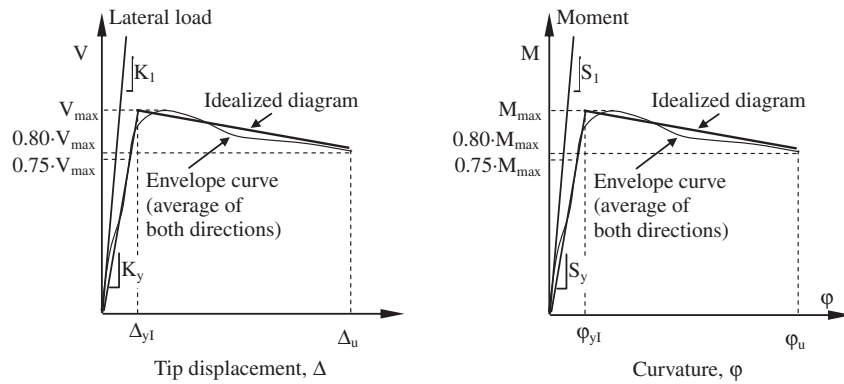


Fig. 13. Ideal curve definitions.

Table 5
Experimental results.

Id	Specimen	φ_{yI} ($\times 10^{-3}$ rad/m)	φ_u ($\times 10^{-3}$ rad/m)	$\mu_{\varphi u}$	Δ_{yI} (mm)	Δ_u (mm)	$\mu_{\Delta u}$	Displacement ductility (NCSR-02)	M_{max} (m kN)	M_{max}/M_{EC-2}	V_{max} (kN)	V_{max}/V_{EC-2}
N1	HF00L05V2S100	17.82	42.18	2.37	11.77	20.64	1.75	No ductility	114.63	1.22	133.25	1.41
N2	HF00L05V2S50	15.64	45.98	2.94	9.41	17.83	1.89	No ductility	90.17	0.92	106.99	1.10
N3	HF00L05V1S50	17.27	73.77	4.27	18.75	66.60	3.55	Medium	65.59	0.96	84.47	1.06
N4	HF00L10V1S70	13.14	67.18	5.11	24.96	91.05	3.65	Medium	18.36	0.99	17.76	1.34
N5	HF30L05V2S600	16.02	32.27	2.01	12.98	18.12	1.40	No ductility	118.27	1.15	138.83	1.33
N6	HF60L05V2S100	15.53	54.11	3.48	13.64	26.27	1.93	No ductility	123.39	1.18	145.51	1.39
N7	HF60L05V2S50	24.95	106.09	4.25	12.63	32.28	2.56	Low	111.47	1.04	123.78	1.15
N8	HF60L05V2S600	17.97	47.60	2.65	14.60	22.25	1.52	No ductility	118.66	1.13	136.29	1.29
N9	HF60L05V1S50	21.00	103.82	4.94	24.42	82.66	3.38	Medium	78.37	0.89	94.87	0.90
N10	HF60L10V1S70	17.03	74.97	4.40	16.96	63.92	3.77	Medium	19.73	0.83	20.16	1.06
N11	HF60L10V2S70	8.05	35.90	4.46	12.80	35.94	2.81	Low	32.41	1.09	24.77	–
N12	NF00L05V2S100	18.57	69.15	3.72	11.48	31.20	2.72	Low	71.68	1.01	85.81	1.11
N13	NF30L05V2S100	13.51	63.95	4.74	10.91	34.93	3.20	Medium	71.25	0.99	80.97	1.02
N14	NF60L05V2S100	20.79	112.34	5.40	11.43	38.57	3.37	Medium	70.83	0.96	83.79	1.06
N15	NF60L05V2S600	22.95	75.59	3.29	14.48	31.42	2.17	Low	71.24	0.98	85.75	1.03

maximum stirrup spacing of $6 \cdot \phi_t$, which is not dependent on ductility. It is interesting to note that for the most restrictive limitation ($6 \cdot \phi_t$), ACI-318 (08) [1] remains on the unsafe side (Table 4) for $\phi_t = 12$ mm and $s_t = 50$ mm ($< 6 \cdot \phi_t = 72$ mm). Furthermore, none of these codes take into account the fact that the separation depends on the type of concrete (NSC or HSC) and the steel fiber content. Therefore, it is necessary to perform further experimental tests. These experimental tests could be used to validate an analytical model to take into account the interaction between the cover spalling and the concrete core induced by transverse steel stirrups and steel fibers, and also the buckling of longitudinal reinforcing bars. Furthermore, these results could be used to verify the stability condition [8].

3.2. Ductility

The ductility parameters were obtained from the idealization of the real envelope diagram, see Fig. 13 [26,16,6]. The elastic branch intersects with the real envelope curve ($V - \Delta$ or $M - \varphi$) up to 75% of V_{max} or M_{max} . The ultimate displacement (Δ_u) or the ultimate curvature (φ_u) in the real envelope curve correspond to the situation of conventional failure (20% loss of capacity), or the maximum displacement or curvature recorded if there was no such loss. Both the lateral load V_u and the bending moment M_u are obtained by imposing energy equilibrium between the idealized bilinear diagram and the real envelope curve. The ultimate displacement ductility is defined as $\mu_{\Delta u} = \Delta_u / \Delta_{yI}$; and the ultimate curvature ductility is defined as $\mu_{\varphi u} = \varphi_u / \varphi_{yI}$.

Table 5 shows the results of ductility in the specimens. Furthermore, the level of ductility reached based on the classification of the Spanish seismic code NCSR-02 [23] is included: high ductility ($\mu_{\Delta u} \geq 4$), medium ductility ($4 > \mu_{\Delta u} \geq 3$), low ductility ($3 > \mu_{\Delta u} \geq 2$), or no ductility ($2 > \mu_{\Delta u} \geq 1$). It can be observed that: (a) HSC specimens without steel fibers, for $\nu = 0.10$ show medium levels of ductility, while for $\nu = 0.35$ there is no ductility; (b) HSC specimens with steel fibers, for $\nu = 0.10$ show medium levels of ductility; for $\nu = 0.35$, with $s_t = 50$ mm show low level, and with $s_t = 100$ mm or 600 mm show no ductility; (c) NSC specimens without fibers, for $\nu = 0.35$ show low ductility; (d) NSC specimens with fibers show medium ductility, except for specimens with $s_t = 600$ mm which have low ductility. It has been seen that minimum transverse reinforcement spacing is required in order to prevent the longitudinal reinforcement in compression from buckling. In the case of stirrup spacing greater than this minimum the inclusion of steel fibers does not improve column ductility.

With the exception of nonfibrous specimens with $\nu = 0.10$, the EC-8 [13] conservative expression that relates both types of ductility ($\mu_{\varphi u} = 2\mu_{\Delta u} - 1$) is fulfilled.

3.3. Strength capacity

Table 5 shows the maximum lateral load (V_{max}) and the maximum bending moment in the critical section (M_{max}). In both cases, the effects of self-weight and second-order effects (for the calculation of the bending moment) have been considered.

4. Analysis of results

4.1. Effects of confinement and inclusion of steel fibers

Fig. 14 shows the results for the analysis of the effects of confinement and the inclusion of fibers. Ductility (μ_{Au} , $\mu_{\phi u}$), and strength capacity (V_{max} , M_{max}) are evaluated as a function of the residual tensile strength f_{R3} . There are six specimens for comparison: HF00L05V2S50, HF60L05V2S50, HF00L05V2S100, HF60L05V2S100, HF30L05V2S600, and HF60L05V2S600. The numerical results are shown in Table 5.

For all the specimens selected, slenderness is 5.77, average concrete compressive strength 73.52 MPa, and average relative normal force 0.34. The values are presented as a function of the transverse reinforcement spacing: 600, 100, and 50 mm. This corresponds to confinement effectiveness factors of 0.01, 0.02, and 0.05 respectively. Moreover, Fig. 14b shows the predicted ductility according to EC-8[13]:

$$\mu_{\phi u} = \frac{\alpha \cdot \omega_{\omega} + 0.035}{30 \cdot v_d \cdot \varepsilon_{sy,d}} \frac{b_o}{b_c} \quad (2)$$

where v_d is the reduced axial compressive force, $\varepsilon_{sy,d}$ is the deformation in the steel for the design stress f_y , b_c is the width of the cross-section, and b_o is the width of the confined core (to the centerline of the hoops). Safety factors are taken to equal one.

The displacement ductility increases with the confinement effectiveness factor, as predicted (Fig. 14a). Thus, in nonfibrous specimens with double transverse reinforcement ratio there was a 30% increase in the displacement ductility (HF00L05V2S100 vs.

HF00L05V2S50). The series corresponding to $\alpha \cdot \omega_{\omega} = 0.02$ ($s_t = 100$ mm) shows that steel fibers improve the deformation capacity of the specimen (HF00L05V2S100 vs. HF60L05V2S100) by 10%. Steel fibers improve concrete post-peak behavior, and delay the effect of concrete spalling.

For $\alpha \cdot \omega_{\omega} = 0.05$ ($s_t = 50$ mm) series, 60 kg/m³ of fibers show a 42% improvement in ductility, HF00L05V2S50 (Fig. 10c) vs. HF60L05V2S50 (Fig. 10d). In this case, steel fibers improve post-peak behavior. The longitudinal reinforcement in compression does not suffer buckling for specimen HF00L05V2S50, while buckling does occur for HF60L05V2S50, where the deformation of the bar in compression is the greatest at failure. Steel fibers increase the bending curvature in the sections included in the plastic hinge, and also the deformation of the compressed reinforcement, in comparison to the nonfibrous specimen. The stiffness of the rebar in compression decreases significantly, and buckling occurs as a result of concrete spalling.

Moreover, specimens HF30L05V2S600 ($s_t = 600$ mm and 30 kg/m³ of fibers) and HF60L05V2S600 ($s_t = 600$ mm and 60 kg/m³ of fibers) have no ductility (μ_{Au} is 1.4 and 1.52 respectively). In this case, the possible beneficial effect of the fibers does not occur because of the compression reinforcement buckling (Fig. 12c).

The curvature ductility ($\mu_{\phi u}$) shows the same tendency as the displacement ductility μ_{Au} (Fig. 14a and b). In this case fibers improve the curvature ductility by more than 40% for 100 and 50 mm transverse reinforcement spacing. This value is on the safe side compared with the predicted value of ductility as stated in EC-8 [13], which does not take into account the favorable effect of the inclusion of steel fibers into the concrete mixture. Since the ideal elastic curve (ϕ_{yi}) of all specimens is almost the same, the increase

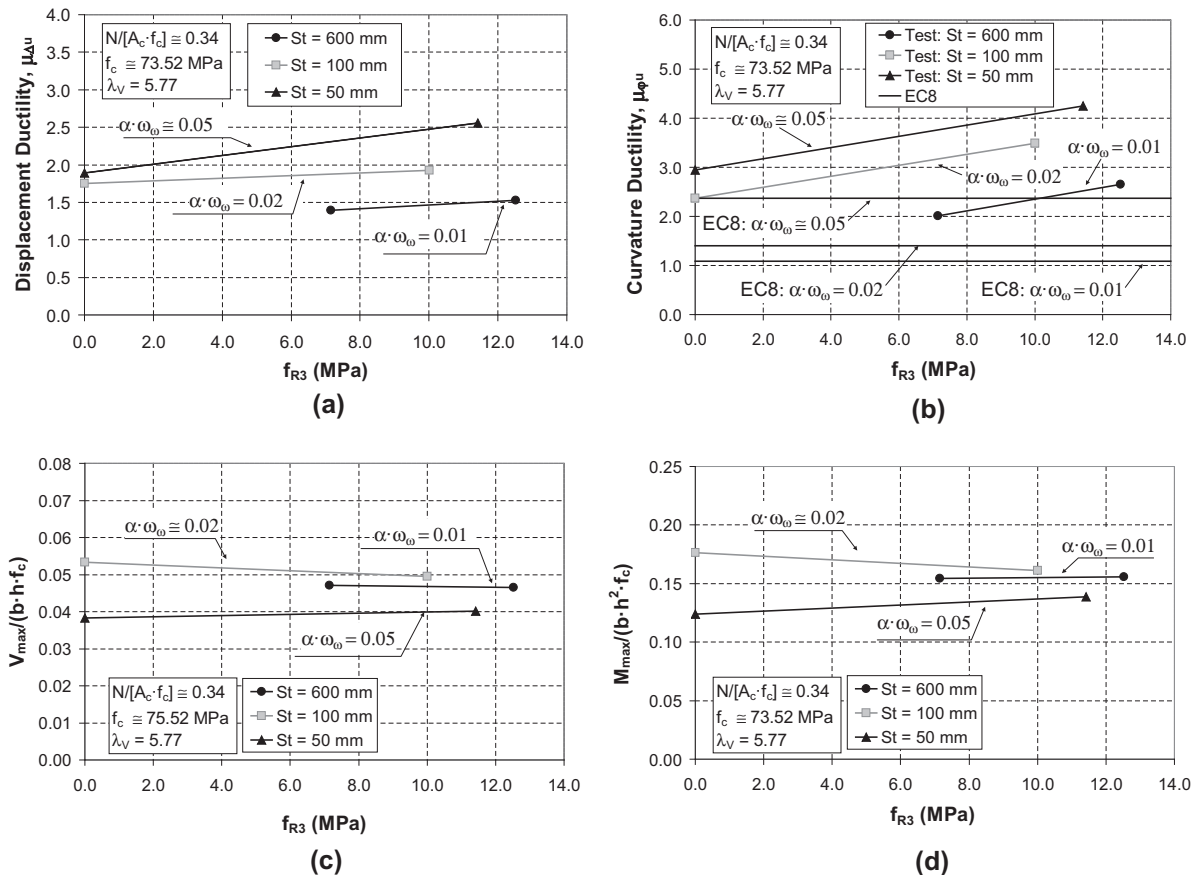


Fig. 14. Deformation and strength capacity: effect of transverse reinforcement and steel fibers.

in $\mu_{\phi u}$ is due to the increase in the ultimate curvature (ϕ_u), which occurs thanks to the improvement in the concrete post-peak behavior.

The mean value of the nondimensional lateral load $V_{max}/(b \cdot h \cdot f_c)$ is 0.05 with a CV = 12% for the 7 specimens analyzed (Fig. 14c). The scatter of the results is reasonable in this type of laboratory test. Consequently, no significant variation is found in the lateral load due to the confinement or the inclusion of steel fibers.

Finally, the mean value of the nondimensional ultimate bending moment, $M_{max}/(b \cdot h^2 \cdot f_c)$ is 0.15 with CV = 12% for all 7 specimens analyzed (Fig. 14d). The scatter of results is reasonable for this type of test. Results show the same tendency as for the case of maximum load. Moreover, the ultimate bending moment does not increase due to the effect of confinement or the inclusion of fibers.

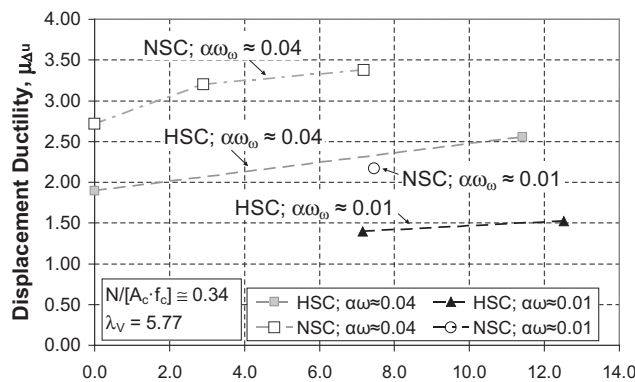
4.2. Effect of concrete strength

Fig. 15 shows the results for the analysis of the effect of the concrete strength in comparison with the deformation capacity (μ_{Au} , $\mu_{\phi u}$), and the strength capacity (V_{max} , M_{max}) as a function of residual tensile strength f_{R3} . All specimens have a slenderness of 5.77 and are subjected to a relative normal force of 0.34. The following specimens are analyzed: four HSC specimens, one without fibers (HF60L05V2S50) and three with fibers (HF60L05V2S50, HF30L05V2S600 and HF60L05V2S600), and four NSC specimens, one without fibers (NF00L05V2S100) and three with fibers (NF30L05V2S100, NF60L05V2S100 and NF60L05V2S600). The numerical results are shown in Table 5. In all cases results are

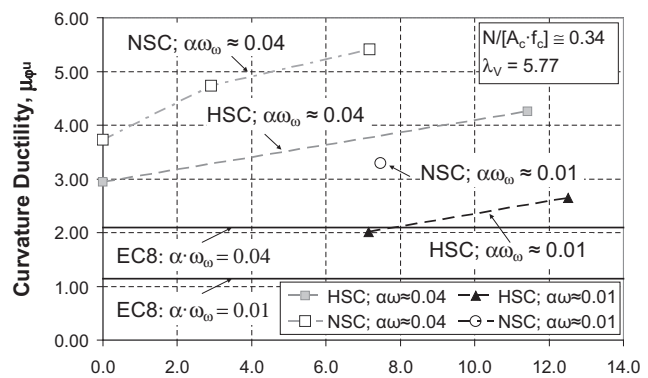
presented by type of concrete (NSC or HSC), and by level of confinement ($\alpha \cdot \omega_{co}$, 0.01 and 0.04). Furthermore, the value of ductility according to Eq. (2) is shown in Fig. 15b.

For the same level of confinement $\alpha \cdot \omega_{co}$ the displacement ductility (μ_{Au}) registered in the NSC specimens is higher than in the HSC ones (Fig. 15a). In the analysis of the series corresponding to a level of confinement $\alpha \cdot \omega_{co}$ of 0.04 (with $s_t = 100$ mm for NSC and $s_t = 50$ mm for HSC) it can be observed that HSC specimens are less ductile than NSC. This happens despite there being a greater possibility of buckling of the longitudinal reinforcement in compression in NSC due to a major transverse reinforcement spacing s_t . In both cases the inclusion of steel fibers improved ductility (Figs. 10 and 15a) for 60 kg/m^3 in by more than 40% for HSC and by 25% in NSC. The favorable effect of steel fibers is more evident in HSC than NSC since HSC is more brittle than NSC (Fig. 10a and c). It is worth noting that HSC specimen HF60L05V2S50 shows a level of ductility similar to that of NSC NF00L05V2S100. Therefore, similar levels of ductility to those of NSC can be achieved in HSC by including steel fibers. Regarding the specimens with $s_t = 600$ mm ($\alpha \cdot \omega_{co} = 0.01$) for NSC and HSC the favorable effect of the fibers does not occur as the buckling of the longitudinal reinforcement in compression results in a significant loss of load capacity (Fig. 12c and f).

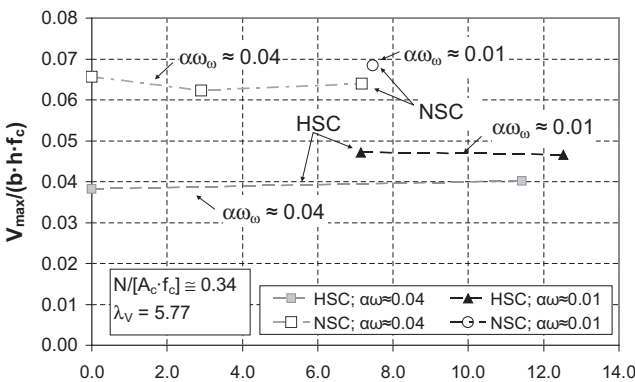
The curvature ductility ($\mu_{\phi u}$) shows approximately the same tendency as the displacement ductility (μ_{Au}) (Fig. 15a and b). For all specimens, maintaining the same parameters, NSC specimens show a curvature ductility 25% greater than that of HSC. The inclusion of steel fibers has resulted in an increase of over 45% of



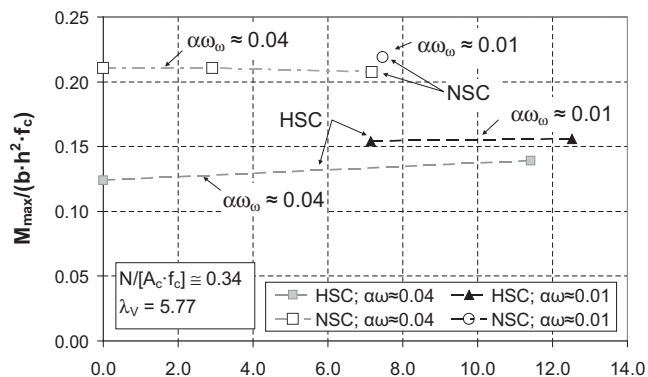
(a)



(b)



(c)



(d)

Fig. 15. Deformation and strength capacity: effect of concrete strength.

ductility for a fiber content of 60 kg/m³ in both NSC and HSC, and $\alpha \cdot \omega_{\omega} = 0.04$.

In theory, according to EC-8 [13], Eq. (2), the curvature ductility does not depend on the type of concrete. However, the curvature ductility achieved is different in HSC and NSC nonfibrous specimens. Regarding the comparison with the predicted values of ductility according to EC-8 [13] it can be observed that this code remains on the safe side.

The nondimensional lateral load $V_{max}/(b \cdot h \cdot f_c)$ does not show a significant variation as a result of the effect of confinement or the inclusion of steel fibers (Fig. 15c), for NSC (mean value = 0.07, CV = 4.09%) or for HSC (mean value = 0.04, CV = 10.41%).

Regarding the nondimensional ultimate bending moment $M_{max}/(b \cdot h^2 \cdot f_c)$, the results obtained show the same tendency as for the nondimensional lateral loads. Thus, for NSC (mean value = 0.217, CV = 2.26%) and for HSC (mean value = 0.14, CV = 10.40%) the ultimate bending moment does not increase due to the effect of the confinement or the inclusion of steel fibers. In both cases, it was observed that after spalling of concrete cover, the capacity of the confined core is less than the capacity of the full unconfined section. Moreover, the longitudinal reinforcement is in tension at failure when the bending moment is maximum, and there is no evidence of a significant improvement in the strength of the section due to tensile residual strength produced by fibers.

This means the use of HSC including steel fibers (steel-fiber-reinforced high-strength concrete, SFRHSC) with suitable positioning of transverse reinforcement can allow the design of columns with a strength capacity greater than that of NSC. Consequently,

SFRHSC could be considered to be preferable to NSC in terms of structural safety in areas with low to medium seismicity. However, codes do not take this favorable effect into account for NSC or for HSC. A more exhaustive study is required to assess the benefits when using this type of concrete.

4.3. Effect of axial load and column slenderness

Fig. 16 shows the results for the analysis of the effect of the axial load and the column slenderness in comparison with the deformation capacity ($\mu_{Au}, \mu_{\phi u}$), and the strength capacity (V_{max}, M_{max}) as a function of the relative normal force $N/(b \cdot h \cdot f_c)$. The results corresponding to specimens with no fibers and with 60 kg/m³ of fiber content are presented. The following specimens are analyzed: three without fibers (HF00L05V2S50, HF00L05V1S50 and HF00L10V1S70), and four with fibers (HF60L05V2S50, HF60L05V1S50, HF60L10V1S70 and HF60L10V2S70). The numerical results are shown in Table 5. Results are presented by type of concrete (with or without fibers) and by column slenderness. Furthermore, the value of ductility according to Eq. (4) is shown in Fig. 16b.

The effect of the axial load in comparison to the displacement ductility μ_{Au} is analyzed (Table 5 and Fig. 16a). It can be observed that ductility decreases in HSC columns with the axial load level for fibrous and nonfibrous specimens and for any column slenderness. In addition, fibrous columns suffered lower losses of ductility for higher axial load levels. It is also worth noting that previous researchers [20,34,3] found that ductility decreases with the axial

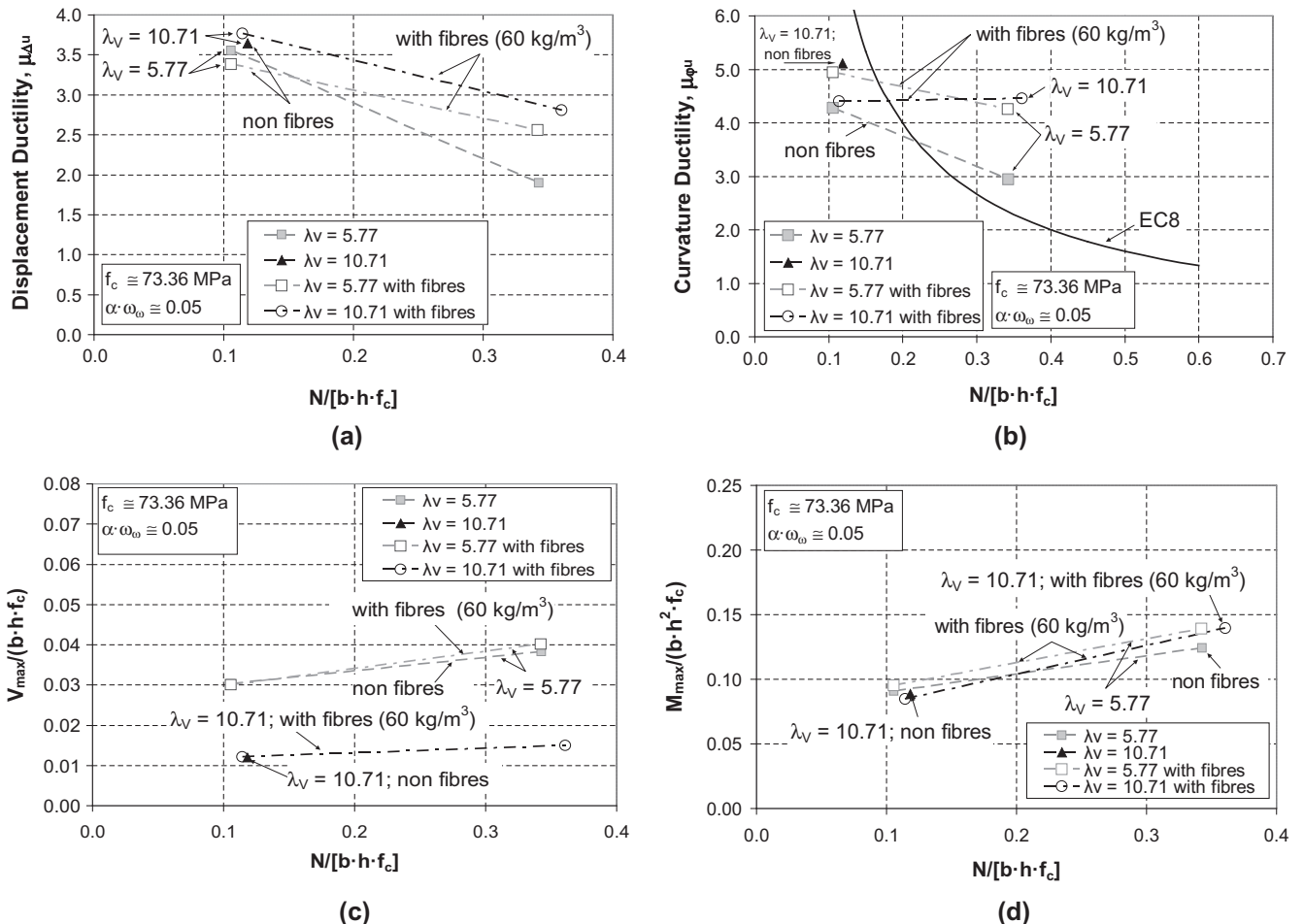


Fig. 16. Deformation and strength capacity: effect of slenderness, axial load level and steel fibers.

load level in nonfibrous HSC columns with low slenderness ($\lambda_v < 6.5$). This is also observed when analyzing curvature ductility (Table 5).

On the other hand, it can be observed that the displacement ductility μ_{Au} depends significantly on the slenderness (Fig. 16a), so that the most slender columns have a greater deformation capacity.

Although a greater column slenderness decreases the load capacity of the column due to second-order effects, its deformation capacity increases and a major ultimate displacement (Δ_u) can be achieved. The analysis of the effect of the slenderness requires further research given the lack of experimental tests available on columns with values of slenderness over 6.5.

Regarding the comparison with EC-8 [13] it is observed that (Fig. 16b): (a) for low axial load levels, with or without steel fibers, the expression included in the code is on the unsafe side; (b) for the case of $\nu = 0.35$, the prediction is adequate for nonfibrous specimens, while it is too conservative for fibrous specimens.

Regarding the maximum load and the ultimate bending moment (Fig. 16c and d), a similar strength capacity is found in specimens with and without fibers when other parameters are kept constant. The other tendencies are as expected when the longitudinal reinforcement ratio, the slenderness, and the axial load level vary.

5. Validation of simplified methods

A comparison was carried out between the experimental results and the method proposed by EC-2 [12].

EC-2 [12] recommends the use of the moment magnification method, which is based on the following factor δ_{ns} to take second-order effects into account.

$$\delta_{ns} = 1 + \frac{\beta}{N_{cr}/N - 1} \quad (3)$$

where $\beta = \pi^2/12$ for a symmetric triangular distribution of the first-order moment, N is the design value of axial load, N_{cr} is the buckling load, which is equal to $\pi^2 \cdot EI/l_p^2$ where EI is the nominal stiffness of the column and l_p is the effective buckling length. The nominal stiffness of the column EI is evaluated according to expression 5.21, section 5.8.7.3 EC-2 [12]. The semi-column is considered as a cantilever column 1.5 m long (Fig. 1) and with an effective length $l_p = 3$ m.

The parabola-rectangle diagram for concrete in compression was used [12] to evaluate the ultimate bending moment resisted by the section, no safety factors were considered. EC-2 [12] does not take into account the effect of the residual tensile strength of the steel fibers in the evaluation of the ultimate bending moment. However, given the fact that the formulation included in MC [18] is the same as in EC-2 [12], and that the former includes the effect of the steel fibers using the rectangular method, MC [18] was used in the validation.

Tables 5 and 6 show the results obtained for all the specimens both for the maximum bending moment M_{max} and for the maximum lateral load V_{max} . It has not been possible to obtain the maximum lateral load V_{max} for specimen HF60L10V2S70 because the

axial load achieved was greater than the buckling load N_{cr} obtained the simplified method.

The prediction of the maximum bending moment (M_{max}) of EC-2 [12] is fairly accurate for NSC, and remains on the safe side for HSC, with a high coefficient of variation in HSC. The following specimens are significantly on the unsafe side (Table 5): HF60L05V1S50 and HF60L10V1S70. This result was expected in the specimens with steel fibers subjected to low axial load levels, given that the steel fibers did not improve the flexural capacity (Figs. 14d, 15d, and 16d). For all tests, the average ratio is 1.03 and the coefficient of variation is 11.47%. Regarding the maximum load capacity obtained from EC-2 [12], the average ratio is 1.12 and the coefficient of variation is 15.55%. Once again, the specimens that remain significantly on the safe side are HF60L05V1S50 and HF60L10V1S70.

6. Conclusions

The following conclusions are drawn in this study:

- The inclusion of steel fibers for NSC and HSC delays concrete cover spalling, the buckling of the longitudinal reinforcement bars in compression, and reduces the critical region length, as there is minor damage in the area where the plastic hinge is likely to occur. There is an improvement in curvature and displacement ductility.
- There is no significant increase in the maximum load capacity with the inclusion of steel fibers, for NSC or for HSC. This suggests that the favorable effect of the residual tensile strength f_{R3} decreases with the application of the cyclic loads.
- The ultimate displacement ductility μ_{Au} increases with the level of confinement, the steel fiber content, and the column slenderness, and with a decrease in the axial load level and the concrete strength. The ultimate curvature ductility $\mu_{\phi u}$ increases with the level of confinement, the steel fiber content, and with a decrease in the axial load level and the concrete strength.
- In HSC columns, a suitable positioning of the transverse reinforcement and the inclusion of steel fibers (SFRHSC) make it possible to reach levels of deformation capacity (ductility) similar to those of NSC. However, codes such as EC-8 [13] do not take this favorable effect into account. Accordingly, further study is required to assess the benefits of the use of SFRHSC concrete in low to medium seismic areas.
- To ensure the required deformation capacity it is necessary to prevent the longitudinal reinforcement in compression from buckling along the length where a plastic hinge may be developed. To this end, an appropriate transverse reinforcement spacing depending on the level of axial load, the type of concrete (NSC or HSC, with or without fibers), the required deformation capacity, and the diameter of the longitudinal reinforcement must be fixed. The codes do not take these parameters into account. To give recommendations and design rules, further experimental and numerical studies should be carried out. In these studies we should consider the interaction between transverse reinforcement and steel fibers.
- The ratio between the critical region length and the total depth of the section l_{cr}/h in HSC columns increases with the column slenderness, the axial load level, and the transverse reinforcement spacing. Similar l_{cr}/h ratios are obtained for NSC and HSC assuming the same parameters in both cases.
- EC-8 [13] ductility predictions are on the safe side for medium axial load levels, but on the unsafe side for low axial load levels, and are conservative for fibrous specimens.
- Finally, the experimental results obtained were compared with the method proposed in EC-2 [12]. The accuracy of this method in predicting the ultimate bending moment is adequate, except

Table 6
Average values. Comparison of experimental values and EC-2 (2004).

	M_{max}/M_{EC-2}		V_{max}/V_{EC-2}	
	Average	CV (%)	Average	CV (%)
NSC without fibers	1.01	–	1.11	–
NSC with fibers	0.98	1.45	1.04	1.80
HSC without fibers	1.04	13.69	1.13	17.24
HSC with fibers	1.06	13.48	1.16	19.35
All	1.03	11.47	1.12	15.55

in the cases of fibrous specimens subjected to low axial load levels whose predicted values remain unsafe. The prediction of the maximum load is more conservative with a high coefficient of variation.

Acknowledgments

The authors of this work wish to thank the research bureau of the Spanish Ministry of Economy and Competitiveness and the Plan E, for the funding of the Project BIA 2008-03734 and BIA 2009-10207.

References

- [1] ACI 318-08. Building code requirements for reinforced concrete. American Concrete Institute, Detroit; 2008. p. 471.
- [2] Aoude H, Cook WD, Mitchell D. Axial load response of columns constructed with fibers and self-consolidating concrete. *ACI Struct J* 2009;106(03):349–57.
- [3] Bae S, Bayrak O. Seismic performance of reinforced concrete columns: P – Δ effect. *ACI Spec Publ* 2006;236:61–80.
- [4] Barrera AC, Bonet JL, Romero ML, Miguel PF. Experimental tests of slender reinforced concrete columns under combined axial load and lateral force. *Eng Struct* 2011;33(12):3676–89.
- [5] Berry M, Parrish M, Eberhard M. PEER structural performance database user's manual. Pacific Earthquake Engineering Research Center, University of California, Berkeley; 2004 <www.ce.washington.edu/~peer1>.
- [6] Caballero-Morrison KE, Bonet JL, Navarro-Gregori J, Martí-Vargas JR. Behaviour of steel fibre – reinforced normal – strength concrete slender columns under cyclic loading. *Eng Struct* 2012;39:162–75.
- [7] Campione G, Mindess S, Zingone G. Compressive stress–strain behaviour of normal and high strength carbon fibre concrete reinforced with spirals. *ACI Mater J* 1999;96(1):27–34.
- [8] Campione G, Fossetti M, Papia M. Behavior of fiber-reinforced concrete columns under axially and eccentrically compressive loads. *ACI Struct J* 2010;107(03):272–81.
- [9] CEB-FIP, Bulletin 25. State of art report (displacement-based seismic design of reinforced concrete buildings). Task Group 7.2, Mayo 2003, Lausanne – Switzerland; 2003.
- [10] Collins Michael P, Mitchel Denis, Macgregor James G. Structural design considerations for high-strength concrete. *Concr Int* 1993:27–34.
- [11] Comisión Permanente del Hormigón. Code on structural concrete EHE-08. Ministerio de Fomento.
- [12] European Committee for Standardization. Eurocode 2: design of concrete structures – Part 1: General rules and rules for buildings. EN 1992-1-1; December 2004.
- [13] European Committee for Standardization. Eurocode 8: design of structures for earthquake resistance – Part 1: General rules, seismic actions and rules for buildings. EN 1998-1; 2004. p. 232.
- [14] Federal Emergency Management Agency, FEMA-P-750. NEHRP recommended provisions for new buildings and other structures. Washington, DC; 2009.
- [15] Foster SJ. On behaviour of high-strength concrete columns: cover spalling, steel fibers and ductility. *ACI Struct J* 2001;98(04):583–9.
- [16] Ho JCM, Pam HJ. Inelastic design of low-axially loaded high-strength reinforced concrete columns. *Eng Struct* 2003;25:1083–96.
- [17] Hsu LS, Hsu CT. Stress–strain behavior of steel fiber high strength concrete under compression. *ACI Struct J* 1997;97(4):448–57.
- [18] International Federation for Structural Concrete (fib). Model code 2010. First complete draft. Bulletin 55 and 56; March 2010.
- [19] Khoury SS, Sheikh SA. Behavior of normal and high strength confined concrete columns with and without stubs. Research report no. UHCEE 91-4, University of Houston, Houston, TX; December; 1991. 345 pp.
- [20] Légeron F, Paultre P. Behavior of high-strength concrete columns under cyclic flexure and constant axial load. *ACI Struct J* 2000;97(4):591–601.
- [21] Li B, Park R, Tanaka H. Effect of confinement on the behaviour of high strength concrete columns under seismic loading. In: *Proceeding Pacific conference on earthquake engineering, New Zealand; 1997. p. 67–78.*
- [22] Mansur MA, Chin MS, We TH. Stress – strain relationship of high strength fibre concrete in compression. *J Mater Civil Eng* 1999;11(1):21–9.
- [23] Ministerio de Fomento. Norma de construcción sismorresistente: parte general y edificación (NCSR-02). RD 997/2002.
- [24] Pam HJ, Ho JCM. Length of critical region for confinement steel in limited ductility high-strength reinforced concrete columns. *Eng Struct* 2009;31:2896–908.
- [25] Panagiotakos TB, Fardis MN. Deformations of reinforced concrete members at yielding and ultimate. *ACI J Struct* 2001;98(2):135–48.
- [26] Paultre P, Légeron F, Mongeau D. Influence of concrete strength and transverse reinforcement yield strength on behavior of high-strength concrete columns. *ACI Struct J* 2001;98(4):490–501.
- [27] Paultre P, Eid R, Langlois Y, Lévesque Y. Behaviour of steel fiber-reinforced high-strength concrete columns under uniaxial compression. *ASCE J Struct Eng* 2010;136(10):1225–35.
- [28] Priestley MJN, Park R. Strength and ductility of concrete bridge columns under seismic loading. *ACI Struct J* 1987;84:6176.
- [29] Sharma UK, Bhargava P, Sheikh SA. Tie-confined fibre-reinforced high strength concrete short columns. *Mag Concr Res* 2007;59(10):757–69.
- [30] UNE-EN 10002-1. Metallic materials. Tensile testing. Part 1: Method of test at ambient temperature. AENOR. Spanish Association for Standards and Certification; July 2002.
- [31] UNE-EN 12390-3. Ensayos de hormigón endurecido – Parte 3: Determinación de la resistencia a compresión de probetas. Asociación española de normalización y certificación, AENOR; December 2000.
- [32] UNE-EN 14651:2007. Método de ensayo para hormigón con fibras metálicas. Determinación de la resistencia a la tracción por flexión (límite de proporcionalidad (LOP), resistencia residual. Asociación española de normalización y certificación, AENOR; September 2007.
- [33] UNE-EN 197-1:2000. Cemento – Parte 1: Composición, especificación y criterio de conformidad para cementos comunes. Asociación española de normalización y certificación, AENOR. Diciembre; December, 2000.
- [34] Wang Q, Zhao G, Lin L. Effect of axial load ratio and stirrups volume ratio on ductility of high-strength concrete columns. *ACI special publication* 149-24, October 1; 1994. p. 433–48.
- [37] Yamashiro R, Siess CP. Moment–rotation characteristics of reinforced concrete members subjected to bending, shear, and axial load. *Civil engineering studies, structural research series no. 260, University of Illinois, Urbana; 1962.*